Time-resolved coherent anti-Stokes Raman-scattering measurements of I_2 in solid Kr: Vibrational dephasing on the ground electronic state at 2.6–32 K

Tiina Kiviniemi, Jukka Aumanen, and Pasi Myllyperkiö
Department of Chemistry, P.O. Box 35, FIN-40014 University of Jyväskylä, Finland

V. A. Apkarian
Department of Chemistry, University of California, Irvine, California 92697-2025

Mika Pettersson[a)]
Department of Chemistry, P.O. Box 35, FIN-40014 University of Jyväskylä, Finland

(Received 4 May 2005; accepted 8 June 2005; published online 18 August 2005)

Time-resolved coherent anti-Stokes Raman-scattering (CARS) measurements are carried out for iodine (I_2) in solid krypton matrices. The dependence of vibrational dephasing time on temperature and vibrational quantum number v is studied. The v dependence is approximately quadratic, while the temperature dependence of both vibrational dephasing and spectral shift, although weak, fits the exponential form characteristic of dephasing by pseudolocal phonons. The analysis of the data indicates that the frequency of the pseudolocal phonons is $\sim 30\ \mathrm{cm}^{-1}$. The longest dephasing times are observed for $v=2$ being ~ 300 ps and limited by inhomogeneous broadening. An increase in the dephasing rate of $v=2$ as the temperature is lowered to $T=2.6$ K is taken as a clear indication of lattice-strain-induced inhomogeneity of the ensemble coherence. © *2005 American Institute of Physics*. [DOI: 10.1063/1.1990115]

I. INTRODUCTION

Optical spectroscopy is a powerful tool to investigate intermolecular interactions in condensed phase. Vibrational spectra, in particular, can give information on the couplings between the molecule and its environment. In frequency domain, this information is contained in the line shape and shift of the frequency. In time domain, the decay of the vibrational coherence with the characteristic time constants can be directly recorded. In principle, the same information can be obtained in both domains and they are related via Fourier transformation. Both energy relaxation and phase relaxation effects contribute to the observables. In a coherent spectroscopic measurement in time domain, the dephasing time (T_2) is measured which, in a homogeneous case, consists of both energy relaxation (T_1) and pure dephasing (T_2') contributions.[1–6] Usually, in condensed media, pure dephasing by the thermal bath dominates. As the temperature of the bath is reduced, energy relaxation can be expected to overtake. Accordingly, measurements as a function of temperature are particularly useful in making mechanistic assignments. In principle, in the limit $T\rightarrow 0$, pure dephasing is suppressed. However, now the possible contribution of sample inhomogeneity must be assessed, and in the absence of methods, such as photon echo which eliminates the inhomogeneous component from observation,[7] inhomogeneous contributions must be extracted from systematics of sample preparation.

The theory of dephasing of electronic or vibrational degrees of freedom in the solid state has been considered within different approaches.[2,4–6,8–13] In the commonly considered limit of weak coupling, perturbative approaches have been extensively employed. Hsu and Skinner have presented a nonperturbative theoretical formulation of the problem.[8–11] The essential results from these theories in the case of weak coupling of the impurity to the host lattice are the following: (i) when the impurity vibration is coupled to lattice phonons, and the Debye density of states is assumed to couple, the T^7 law is obtained, and (ii) when the impurity is coupled to local phonons, an exponential temperature dependence results. For the line shift, exponential temperature dependence has been found for weak coupling.[9,13] In addition, for vibrational overtones, a quadratic dependence of the dephasing rate on the vibrational quantum number v has been obtained, and experimentally observed.[5,14,15] This result has been observed for the liquid phase as well.[16] In some cases, a subquadratic dependence has been observed.[17]

Despite the success of the approximate theories to account for the general behavior of vibrational dephasing, more detailed understanding of the phenomenon is desirable. With the development of the computing resources and methods, accurate quantum simulations of the nuclear degrees of freedom in many-body systems can be performed.[18,19] This can lead to more detailed understanding of dephasing, but suitable model systems are needed to allow rigorous comparisons between simulations and experiments. For the important generalization of an anharmonic oscillator in a bath, an ideal test case is provided by rare-gas solids doped with a diatomic molecule. Recent experiments on time-resolved coherent anti-Stokes Raman scattering (TR-CARS) of iodine in solid

[a)]Author to whom correspondence should be addressed. Electronic mail: mijopett@cc.jyu.fi

argon and krypton have demonstrated that extensive information on the properties of this model system can be obtained.[14,20–22] The dephasing times as a function of temperature and vibrational state have been measured in both solids, thus forming an extensive body of data that can be used to test theories. For experimental reasons, more extensive data have been obtained for iodine in krypton including vibrational states between $v=1$ and 19 temperatures between 7 and 45 K. However, since the CARS method does not discriminate between inhomogeneous and homogeneous contributions to dephasing, the longest observed dephasing times are suspected to be limited by inhomogeneous broadening. Therefore, it would be desirable to extend these measurements to more homogeneous samples. Additionally, it would be interesting to extend the studies to temperatures below 7 K.

In this paper, we report results of femtosecond CARS measurements on matrix-isolated iodine molecules on samples prepared in a different way from those in previous similar experiments. The prepared vibrational coherences contain information on the vibrational states from $v=2$ to 16. Our data show that the inhomogeneous broadening is smaller in the present experiments. Moreover, the study of temperature dependence is now extended down to 2.6 K; and additionally, we report data on the frequency shift as a function of temperature.

II. EXPERIMENTAL DETAILS

The I_2/Kr=1/2600 samples were prepared by the continuous deposition method on a 100-μm-thick sapphire substrate at $T=40$ K. A pumped, liquid-He flow cryostat, which achieves a base temperature of ~2.6 K, is used. After deposition, the sample is cooled slowly (0.5 K/min) to the measurement temperature. The temperature dependence of dephasing times of a given vibrational superposition was measured from a single sample.

To obtain matrices of high optical quality, which is crucial for the success of the TR-CARS experiments, the sample preparation technique was carefully tested by growing samples at different temperatures while monitoring the matrix thickness by using interference of a HeNe laser beam. The scattering properties of the matrix were also inspected both visually and from the transmitted HeNe laser beam. Different growth rates were correlated with the reading of a calibrated needle valve, resulting in a calibration curve that was used in the CARS measurements to determine the sample thickness. Using deposition temperature of 40 K and a deposition rate of ~0.2 mmol/min yields matrices of high optical quality that can be grown to a thickness of at least ~500 μm without significant increase in scattering. The electronic absorption spectrum of I_2 in the visible range was measured during the matrix growth. The spectrum is shown in Fig. 1 together with the corresponding gas-phase data.[23] The spectra are very similar, the matrix spectrum being only slightly shifted and narrower. The monomericity of the sample was tested by resonance Raman measurements with a 532-nm excitation laser (Coherent, Verdi). The spectrum is shown in Fig. 2. It shows mainly a signal from monomeric iodine molecules.[24,25] The broad band appearing as a shoulder at ~180 cm^{-1} does not seem to belong to the dimer as there are no higher vibrational components visible in the spectrum, which is characteristic for iodine dimers.[24,25]

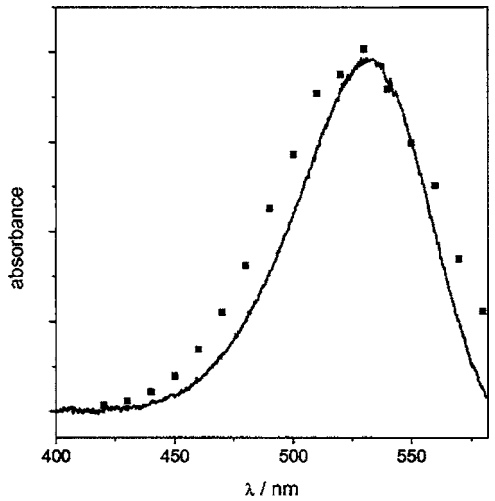

FIG. 1. Absorption spectrum of I_2 in solid Kr (solid line). The gas-phase data from Ref. 23 is marked by dots. The *y* scale is individually scaled for both data.

The CARS setup is shown in Fig. 3. A Coherent Mira Ti:sapphire oscillator and a Quantronix Odin amplifier are used, and the output (800 nm, ~0.8 mJ, and 1 kHz) is used to pump a homebuilt noncollinear optical parametric amplifier (NOPA) and a commercial optical parametric amplifier (OPA) (Topas, Light Conversion Ltd.). The NOPA output pulse with a bandwidth of ~470 cm^{-1} is used as the Stokes pulse. The OPA output is split into two, yielding the pump and probe pulses with a bandwidth of ~340 cm^{-1}. The central wavelengths of the beams are tuned between 600–685 and 565–580 nm for NOPA and OPA, respectively. Two delay lines, for the Stokes and probe beams, are used to control the timing between pulses. The probe delay line is equipped with a stepper motor with a step size of 1 μm, corresponding to a delay of ~6,67 fs. The beams are arranged in a boxcars geometry and a 20-cm focal length achromat lens is used to focus the three beams and to collimate the CARS beam. The intensities of the beams are attenuated to deliver pulse ener-

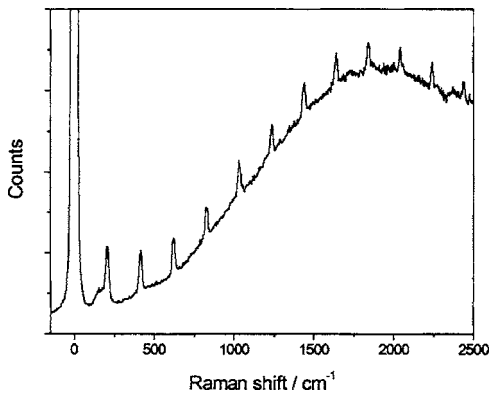

FIG. 2. Resonance Raman spectrum of I_2/Kr matrix grown at 40 K and measured at 4.1 K. Excitation wavelength of 532 nm. The spectrum shows mainly monomeric iodine.

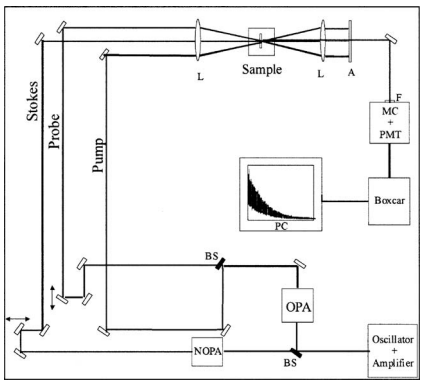

FIG. 3. The experimental setup for the CARS measurements. A Coherent Mira Ti:sapphire oscillator and Quantronix Odin amplifier are used to pump an OPA (Topas, Light Conversion Ltd.) and a homebuilt NOPA. Two delay lines are used to control the timing between the pulses. Achromat lenses (L) are used to focus the three beams to the sample and to collimate the CARS beam. The signal is filtered spatially with an aperture (A), and spectrally with an interference filter (F) and a monochromator (MC) and detected with a cooled photomultiplier tube (PMT). A boxcar integrator is used for the data collection.

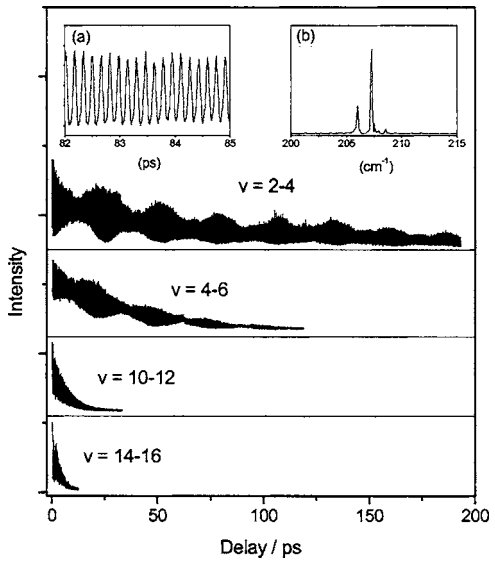

FIG. 4. CARS signals for different vibrational superpositions at $T=20$ K. The different lifetimes of the signals indicate a strong dependence of the dephasing time on the vibrational state. (a) An expanded view of the signal showing the oscillations, (b) a Fourier transform of the $v=2$–4 data. The long dephasing time yields very well-resolved bands in the frequency domain. The center wavelength for pump and probe pulses was 580 nm except in the $v=14$–16 experiment, where 565 nm was used. The center wavelengths for the Stokes pulse were 600 nm ($v=2$–4), 620 nm ($v=4$–6), 660 nm ($v=10$–12), and 685 nm ($v=14$–16). The temporal width of the pulses was ~80 fs for the pump and probe pulses, and ~40 fs for the Stokes pulse.

gies <1 μJ at the sample. Spatial filtering of the CARS signal is achieved with an aperture, and spectral filtering with interference filters and a monochromator. A cooled photomultiplier tube (PMT) is used for detection and a boxcar integrator for data collection. The repetition rate is l kHz, and 100 pulses are averaged for one data point. The pulse energies of all three beams are monitored during measurements, and the data are corrected assuming a linear dependence of the signal on the pulse energy of each beam.

III. EXPERIMENTAL RESULTS

The CARS signals were measured as a function of the probe delay for four different vibrational superpositions on the ground electronic state of I_2 at five different temperatures: 32, 20, 10, 4.1, and 2.6 K. To be clear, the vibrational superposition is created due to the broad bandwidth of the excitation resulting in several Raman transitions being excited simultaneously. Quantum beating between different transitions can be observed as oscillatory structure in the signals. The composition of a superposition depends on temporal excitation pulse widths and frequencies. For example, $\Psi=a|v=2\rangle+b|v=3\rangle$ is referred to as the $v=2+3$ superposition. In a two-state preparation, e.g., $v=2+3$, the single beat at the difference frequency $\omega_{3-2}=\omega_3-\omega_2$ is observed, while for a three-state superposition, e.g., $v=2+3+4$, beside the fundamental beats ω_{3-2} and ω_{4-3} the overtone beat at ω_{4-2} is observed. In Fig. 4, the signal for different superpositions at $T=20$ K is shown. The same scale on x axis for all the data emphasizes a strong dependence of the dephasing times on the vibrational state. The expansion of the signal [inset (a) in Fig. 4] shows a strong modulation of the signal at a period of ~160 fs, corresponding to the vibrational period of the I_2 molecule. The recursion of the signal envelope at an-27-ps period corresponds to the first anharmonicity of the iodine molecule on its ground electronic state. For the superpositions of higher vibrational states ($v>10$), the dephasing times are shorter than the recursion time, and no recursions can be observed within the experimental signal-to-noise ratio.

The frequency domain spectra of the transients were obtained via Fourier transformation of the time domain signal. The region near 200 cm^{-1} from the $v=2+3+4$ superposition is shown in the inset (b) of Fig. 4. The relatively long dephasing times at low vibrational states yield very well resolved bands. At higher vibrational states the bands are not well resolved due to shorter dephasing times, making the analysis of the measurements more difficult. The prepared superpositions contained usually three or four different vibrational states with significant amplitude, resulting in two or three bands in the region near 200 cm^{-1} and one or two bands in the region near 400 cm^{-1} of the frequency domain spectra.

The experimental data were analyzed in both frequency and time domain to obtain the dephasing rates and the vibrational frequencies. In frequency domain, the bands were fitted with Lorentzian line shapes to yield the dephasing rates (γ) from the bandwidth. Both Lorentzian and Gaussian line shapes were tested in the fittings, and the Lorentzian gave usually better fits. These bandwidths and the frequencies of the bands were then used as initial guesses in the time domain fits. For the time domain fits, we used sums of exponentially damped cosines, following the approach of Karavitis and Apkarian:[21]

$$S(t) \propto \sum_{v,v'} c_v c_{v'} \cos(\omega_{v,v'} t + \phi_{v,v'}) e^{-(\gamma_v+\gamma_{v'})t}, \tag{1}$$

where c_v are the amplitudes, $\omega_{v,v'}=\omega_v-\omega_{v'}$ are the frequencies, $\phi_{v,v'}$ the phases, and $\gamma_v \equiv \gamma_{v,0}$ are dephasing rates,

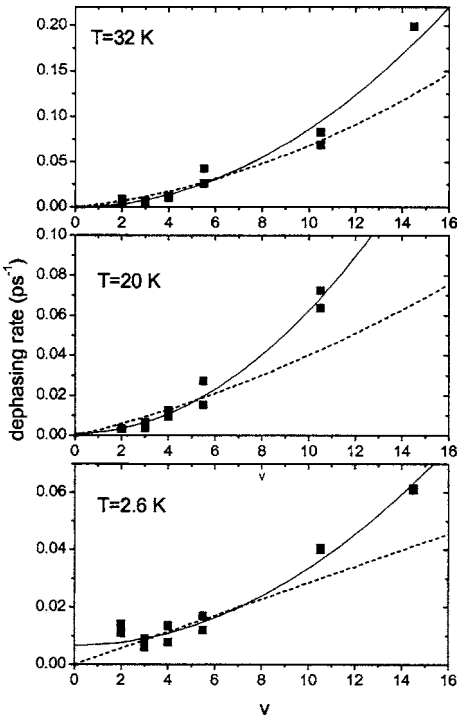

FIG. 5. The dependence of the dephasing rates on the vibrational states at selected temperatures obtained from the time and frequency domain fits of the experimental data. The dashed lines represent the formula derived by Karavitis *et al.* for the v and T dependences of the dephasing rates (Ref. 14). The solid line is a quadratic fit ($\gamma=A+Bv^2$) to the experimental data.

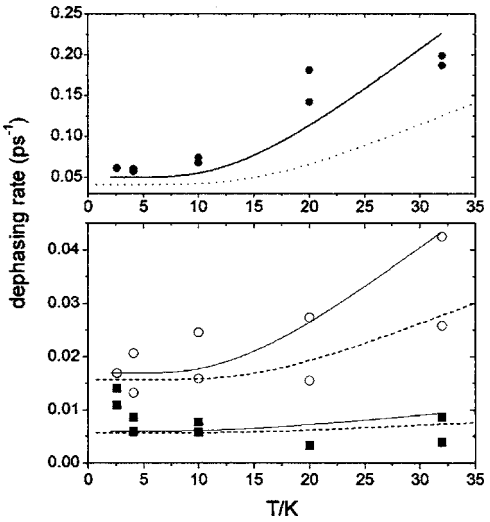

FIG. 6. The temperature dependence of the dephasing rates extracted from the time and frequency domain fits. (■) $v=2$, (○) $v=5,6$ (average), and (●) $v=14,15$ (average). The increase of dephasing rate at 2.6 K for $v=2$ data is due to increased inhomogeneous broadening caused by the change of morphology of the sample upon cooling. The dashed line is the data from Ref. 14. The solid line is the fit according to Eq. (16) (see text).

namely, the decay of amplitude level correlation between state v and $v=0$. The parameters in the fits were not constrained by any functional form, but the condition $\gamma_{v'}>\gamma_v$ for $v'>v$ was imposed. In most cases, however, the individual parameters for each state cannot be obtained reliably, so one to three independent terms were used to obtain average dephasing rates.

The v dependencies of the dephasing rates at three different temperatures, obtained from both the frequency and time domain fits, are collected in Fig. 5. The data do not behave very smoothly, reflecting all the possible error sources in both the measurements and the analysis. Especially at higher vibrational states, fast dephasing results in bands overlapping in the frequency domain, making the analysis more difficult. However, the overall behavior agrees reasonably with the results of Karavitis *et al.*, which is shown in the figure with a dashed line.[14] The dephasing time is shortened by a factor of ~20 in going from $v=2$ to $v=15$. The lowest observed dephasing rate is ~0.003 ps^{-1}, corresponding to an ~0.03-cm^{-1} linewidth in the frequency domain.

The temperature dependence of the dephasing rates is very weak, as can be seen from Fig. 6. A tenfold increase in the temperature induces only an approximately twofold increase in the dephasing rate of states above $v=5$. In the case of the lower-lying vibrational levels, exemplified by $v=2$ in Fig. 6, observed dephasing rate increases as the temperature is lowered. This is the most direct evidence of the inhomogeneous contribution to the measured decay of the ensemble coherence. Cooling the sample below 4.1 K introduces cracks and leads to increased light scattering visible to the eye. The observed inverse T dependence of dephasing rates must be ascribed to strain-induced inhomogeneity of the trapping sites in which the ensemble of molecules is isolated in the polycrystalline matrix. Thus, for the lowest vibrational levels measured, $v=2$, 3, the observed dephasing rate at 2.6 K is determined by the sample morphology, and therefore can be expected to be sensitive to the method of preparation. The T dependence of states above $v=5$ is not inverted as $T\rightarrow 0$ (see Fig. 6), indicating that at least strain-induced inhomogeneity does not play a role in the decay of the prepared vibrational coherence.

Temperature dependence of the beat frequencies was observed at the lowest vibrational states ($v=2$–4), where the bands in the frequency domain are narrow and well resolved. The dependence is shown in Figs. 7 and 8 for the beat frequency ω_{3-2}. The effect is small, ~0.14 cm^{-1} in going from

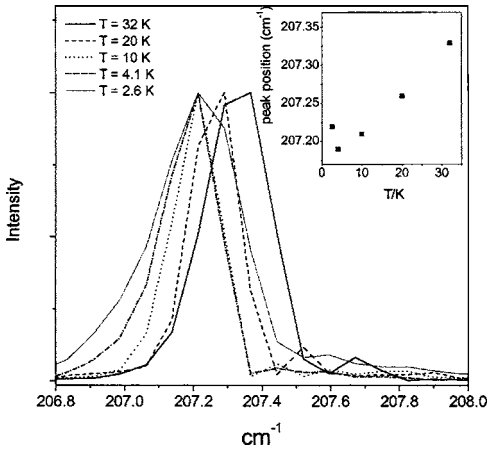

FIG. 7. The effect of temperature on the frequency for the $v=2$–3 transition. The spectra are obtained from the time domain signals by Fourier transformation. The inset shows the shift as a function of temperature. The 2.6-K data point shows anomalous behavior due to the change of morphology of the sample upon cooling.

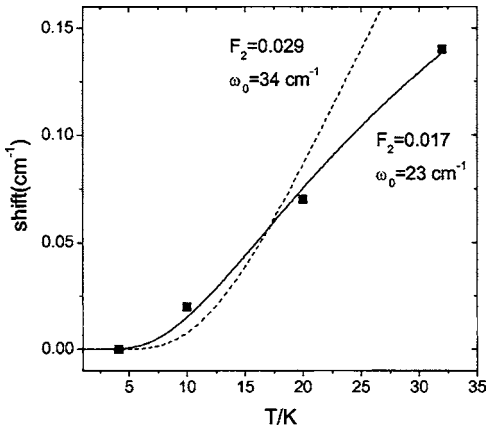

FIG. 8. The frequency of the $v=2$–3 transition as a function of temperature. The 2.6-K data point is omitted (see text for details). The solid line is a fit according to Eq. (17) with parameters marked in the figure. The dashed line is a fit using parameters obtained from the analysis of the dephasing data.

32 to 4.1 K, but detectable. The frequency shifts to lower wave numbers as the temperature is lowered, except at 2.6 K, where the sample deformation, described above, takes place. This frequency shift can also be seen in the Birge-Sponer analysis of the observed frequencies which yields slightly different values for ω_e and $\omega_e\chi_e$ at different temperatures. The values obtained at $T=32$ K, $\omega_e=211.20\pm0.01$ cm^{-1}, and $\omega_e\chi_e=0.642\pm0.001$ cm^{-1} are notably smaller than the corresponding values reported by Karavitis *et al.* ($\omega_e=211.56\pm0.14$ cm^{-1} and $\omega_e\chi_e=0.658\pm0.006$ cm^{-1}).[14] Within the experimental accuracy, this magnitude of variation can be explained by the difference in sample morphology due to different preparation, and by the temperature effect.

IV. DISCUSSION AND ANALYSIS

The preparation method of the sample is described in detail in this report because it differs from the method used in previous similar experiments.[14,20–22] We use continuous deposition and a deposition temperature of 40 K while pulsed deposition and 32 K were used previously. The higher deposition temperature here is expected to yield more homogeneous samples and this is indeed observed in the dephasing times as discussed later. An important finding is that the isolation is very good even at such a high deposition temperature as indicated by the resonance Raman spectrum (see Fig. 2) and the absence of signatures of low-frequency components in the CARS signals. The optical quality of the sample is of importance in CARS measurements and the parameters used in our sample preparation yield matrices of exceedingly good optical properties.

The CARS measurements are carried out along the same lines as in the previous similar measurements and the full account of the theoretical background can be found in Ref. 20, 21, 26, and 27. In short, we prepare a vibrational Raman packet by the pump and Stokes pulses where the pulses are in electronic resonance with the *B-X* transition of iodine molecule. The spectral width and wavelength of the pulses determine the composition of the prepared vibrational coherence. The third "probe" pulse probes the created coherence via emission of a signal photon emitted by the time-dependent third-order polarization. The fast electronic dephasing ensures that the anti-Stokes radiation is emitted only once during the compression of the I–I bond.[20]

Since the wavelength of the Stokes pulse is chosen not to be in strong resonance with the transitions from the ground vibrational and electronic state the polarization consists mainly of one component,

$$P^{(3)}_{\mathbf{k}_{\mathrm{AS}}}(t)=\langle\varphi^{(0)}(t)|\hat{\mu}|\varphi^{(3)}(t)\rangle+\text{c.c.} \tag{2}$$

The detector measures the time- and frequency-integrated signal in the anti-Stokes (AS) direction, $\mathbf{k}_{\mathrm{AS}}=\mathbf{k}_1-\mathbf{k}_2+\mathbf{k}_3$. The indices 1, 2, and 3 refer to the pump, Stokes, and probe pulses, respectively. The signal is recorded with a square-law detector,

$$S(t_{21},t_{32})=\int_{-\infty}^{\infty}dt'|P^{(3)}(t')|^2, \tag{3}$$

where t_{21} is the interval between pump and Stokes pulses and t_{32} is the interval between Stokes and probe pulses. The pump and Stokes pulses nearly overlap in time and the delay time between Stokes and probe pulses is scanned which results in the observed signal.

The measurement yields directly the time correlation function between the initial state (the molecule in $v=0$) and the prepared vibrational coherence. Fitting the signal according to Eq. (1) yields state specific dephasing times and frequencies. Alternatively, the same information may be extracted from the Fourier transform of the measured signal, now in terms of peak positions and linewidths.

Inspection of Fig. 4 shows that the dephasing time is strongly dependent on v in agreement with the previous findings and predictions of theory.[14,21] The inset (b) shows that the bands resulting from different beat frequencies (ω_{3-2} and ω_{4-3}) are clearly resolved in the frequency domain. In order to show this more quantitatively the v dependence of dephasing time is illustrated in Fig. 5 for three different temperatures. For comparison, the results from Ref. 14 are shown in the figure by a dashed line.

Before going to more quantitative analysis we should address the issue of inhomogeneous broadening in order to evaluate the usefulness of the data set. The dephasing rate reaches its lower limit with a value of ~0.003 ps^{-1} as the lowest value in our data. This sets the upper limit of inhomogeneous broadening in our samples. This seems to be somewhat lower than the lowest values reported in Refs. 14 and 21 and thus indicates that the present samples are more homogeneous as expected from the higher deposition temperature. This is also evident by comparing the power spectrum in the inset (b) of Fig. 4 to the Fig. 5 of Ref. 21.

Next, we outline the theoretical framework we use to interpret the results. We use the usual partition of the total system into an anharmonic oscillator which is weakly coupled to a bath of harmonic oscillators. The total Hamiltonian is given by[28]

$$H=H_S+H_B+H_{SB}, \tag{4}$$

$$H_S = \tfrac{1}{4}\hbar\omega_0(p^2+q^2) + V_{\text{anh}}(q), \tag{5}$$

$$H_B = \frac{1}{4}\sum_\alpha \hbar\omega_\alpha^P(P_\alpha^2+Q_\alpha^2), \tag{6}$$

$$H_{SB} = \sum_\alpha A_\alpha(q)Q_\alpha + \frac{1}{2}\sum_{\alpha\beta} U_{\alpha\beta}(q)Q_\alpha Q_\beta. \tag{7}$$

.

H_S is the Hamiltonian for the anharmonic oscillator with a scaled coordinate q and V_{anh} is the anharmonic part of the potential. The bath (H_B) is described as a collection of harmonic oscillators representing the lattice phonons. The interaction potential (H_{SB}) is expanded in a Taylor series and truncated at quadratic order. In order to simplify the description, the bath coordinates are described as a single collective coordinate which is a linear combination of the bath modes.

$$\phi = \sum_\alpha h_\alpha^P Q_\alpha. \tag{8}$$

Then the interaction potential can be written as

$$H_{SB} = A(q)\phi + \tfrac{1}{2}U(q)\phi^2. \tag{9}$$

The linear term in ϕ leads only to a temperature-independent frequency shift and the production of phonon sidebands, while the quadratic term is responsible for dephasing.[28] Dropping the linear term in Eq. (9), the weak-coupling limit of the dephasing rate γ and the shift of the vibrational frequency $\Delta\omega$ of the renormalized system (4)–(9) are obtained,[28]

$$\gamma(v,T) = \frac{W^2}{\pi}\int_0^\infty d\omega n(\omega)[n(\omega)+1]\Gamma_P(\omega)^2, \tag{10}$$

$$\Delta\omega = \frac{W}{\pi}\int_0^\infty d\omega n(\omega)\Gamma_P(\omega), \tag{11}$$

where $n(\omega)$ is the phonon occupation number,

$$n(\omega) = \frac{1}{\exp(\hbar\omega/kT)-1}, \tag{12}$$

and $\Gamma_P(\omega)$ is the phonon spectral density. Its explicit form depends on the coupling between the molecule and phonons. The coupling parameter W is given by

$$W = \langle v|U(q)|v\rangle - \langle 0|U(q)|0\rangle, \tag{13}$$

where v is the quantum number of the vibrational state of the system. In order to calculate W, $U(q)$ should be specified. $U(q)$ is expanded in a Taylor series up to the quadratic term

$$\begin{aligned} U(q) &= U(0) + \left.\frac{\partial U}{\partial q}\right|_0 q + \frac{1}{2}\left.\frac{\partial^2 U}{\partial q^2}\right|_0 q^2 \\ &= U(0) + F_1 q + F_2 q^2. \end{aligned} \tag{14}$$

Now, the expression for W depends on the choice of the system. If the system is harmonic, then the quadratic term gives the only nonzero expectation values. Then combining (13) and (14) and evaluating the expectation values we obtain

$$W = F_2 v, \tag{15}$$

and the working expressions for the dephasing rate and line shift become

$$\gamma(v,T) = \frac{F_2^2 v^2}{\pi}\int_0^\infty d\omega n(\omega)[n(\omega)+1]\Gamma_P(\omega)^2, \tag{16}$$

$$\Delta\omega = \frac{F_2 v}{\pi}\int_0^\infty d\omega n(\omega)\Gamma_P(\omega). \tag{17}$$

Thus, in the harmonic approximation for the system, the dephasing rate is quadratic in v and the line shift is linear in v.

The expressions for anharmonic systems are more involved and lead to more complex v dependence. For the Morse oscillator, both the linear and quadratic terms in q are nonzero, therefore a strictly quadratic v dependence does not hold. Since high-lying vibrations, states up to $v=15$–19, are under consideration, deviations from the harmonic approximation are expected. Thus, since the vibrational level structure is well represented by a Morse oscillator, it is interesting to check the v dependence of the dephasing rate within the theory outlined above. The task is to evaluate the expectation values for q and q^2 for several values of v. The analytical expressions for the expectation values have been derived by Gallas.[29] We have calculated numerically the expectation values up to $v=12$ for a Morse oscillator described by the reduced mass of iodine and ω_e and $\omega_e x_e$ parameters taken from our Birge-Sponer fit for the 32-K data. The results are shown in Fig. 9 as the ratio $\gamma(v)/\gamma(v=1)$ obtained for the linear and quadratic terms alone. Included in the figure is the quadratic v dependence predicted by the harmonic approximation. It can be seen that the linear coupling gives almost quadratic dependence up to $v=12$. The quadratic coupling gives stronger than quadratic dependence of dephasing on v.

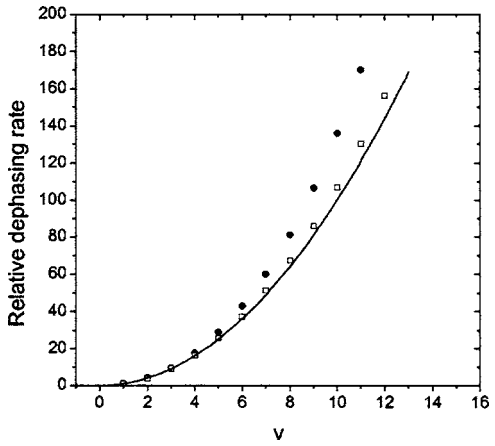

FIG. 9. Calculated dependence of the dephasing rate on the vibrational quantum number v according to Eqs. (10), (13), and (14) for a Morse oscillator with parameters obtained for I_2 in solid Kr (ω_e=211.20 cm^{-1} and $\omega_e x_e$=0.642 cm^{-1}). (□) Linear term q only and (●) quadratic term (q^2) only. The data show the calculated dephasing rate relative to the rate for $v=1$. The solid line is the quadratic dependence characteristic for a harmonic oscillator.

At $v=12$ the dephasing rate would be ~45% higher than what pure v^2 dependence would show. Thus, it is evident that if accurate data are available it should be possible to deduce the dominating term in the expansion (14). In previous studies it was also found that the v dependence is stronger than quadratic for a Morse oscillator.[15] However, in that study, a subquadratic dependence was obtained for linear coupling term while we find slightly stronger than quadratic dependence. The origin of the discrepancy is not clear at the moment.

Now, we are ready to analyze the experimental results in more detail. Since our data are limited to few points, we restrict the analysis to test the quadratic dependence. Although pure homogeneous dephasing vanishes at 0 K we add a constant term to take into account the limit due to inhomogeneous broadening and vibrational relaxation. The results of the fit are shown in Fig. 5 as a solid line showing that the quadratic dependence fits the data reasonably well. This is also in qualitative agreement with previous findings.[14] The lower limit of the dephasing rate is set either by the inhomogeneous broadening or vibrational relaxation but we cannot distinguish unambiguously the contribution of vibrational relaxation from our data. It should be noted that both effects may show linear dependence on v.[14,30] Paige and Harris have measured the vibrational relaxation rate of I_2 in liquid Xe at temperatures between 253 and 323 K.[31] Their results showed that near the bottom of the potential-energy surface the relaxation time is on the order of nanoseconds. Although there is no corresponding data available for solid krypton, the time scale should be roughly similar. Thus, since the longest-observed coherence times in this work are up to several hundred picoseconds, it is possible that there is a contribution from vibrational lifetime in these values. Measurements of vibrational relaxation would be interesting in this regard.

The temperature dependence of the dephasing rate is very weak as seen in Fig. 6. We note here once more that the rise in the dephasing rate with decreasing temperature below 4.1 K is due to the change of morphology of the sample caused by thermal stress which increases the inhomogeneous effects. Therefore, the temperature dependence can be reliably estimated only for temperatures approximately $\geqslant$4.1 K for low vibrational states. By inspection of the data it is hard to reliably judge the functional form of the temperature dependence. We can safely exclude the T^7 dependence within the error limits of the data, thus eliminating the mechanism of dephasing by coupling to extended lattice phonons. On the other hand, the data are in a reasonable agreement with the exponential behavior found in Ref. 14 as shown in Fig. 6 with a dashed line.

It is notable that for the low-lying vibrational states the present measurements are more accurate for measuring the shift in vibrational frequency than the dephasing time. Therefore, it is valuable to measure the shift of the frequency as a function of temperature since within the theory outlined above it depends on the same interactions with phonons as the dephasing rate. Most reliable line-shift measurements can be done for the lowest states that are well resolved in the frequency domain. In Fig. 7 the shift is presented for the beat frequency ω_{3-2}. The temperature dependence is shown in Fig. 8 along with the fit according to Eq. (17). In the fit the spectral density was taken to be Gaussian with a full width at half maximum (FWHM) of 5 cm^{-1} (see later). The 2.6-K data point is excluded from the fit due to broadening and the shift due to the change in the morphology of the sample upon cooling. The fit is reasonably good to establish with higher reliability than the dephasing rate analysis that the dependence is exponential. This is indicative of coupling with pseudolocal phonons. The frequency of the pseudolocal mode obtained from the fit is 23 cm^{-1}.

Finally, we carry out a unified analysis of both dephasing rate and line shift according to Eq. (16) and (17). In Ref. 14, it was concluded that the dephasing is due to coupling with the pseudolocal phonons as evidenced by clear exponential temperature dependence. Our data in Fig. 6 is in line with this, although the quality of data is not sufficient to establish this with confidence. In Ref. 14 the T dependence of the dephasing rate was successfully modeled with Eq. (16) by using the pseudolocal phonon frequency of 34 cm^{-1} and the spectral width of 5 cm^{-1} for a Gaussian-type of spectral density. We used the same parameters to calculate the dephasing rate numerically according to (16) by setting F_2 to 1. Then the value of F_2 was determined so that the quadratic fit of the data at 32 K was reproduced. The obtained value for F_2 is 0.029. It should be noted that for $0\rightarrow1$ transition this value would be equal to the parameter W. As expected, the weak-coupling assumption of $W\ll1$ is valid. The temperature dependencies were then calculated for several states and a reasonably good agreement was obtained for the whole data set. The results are shown in Fig. 6 with a solid line. A further test was then made by calculating with these parameters the temperature dependence of the line shift from (17) and comparing the result with the experimental data. The comparison is shown in Fig. 8 with a dashed line. The agreement is not perfect but reasonably good keeping in mind that the line shift was calculated based only on data obtained from the analysis of the dephasing rate. The fit to the frequency shift alone gave 23 cm^{-1} for the local mode frequency and the true value is probably between this and 34 cm^{-1}, obtained from the analysis of the dephasing rate.

V. CONCLUSIONS

The dephasing of vibrational coherence of matrix-isolated I_2 is studied with time-resolved coherent anti-Stokes Raman scattering. The prepared vibrational superpositions contain information on the states between $v=2$ and 16, and the temperature dependence of dephasing time and frequency shift is studied between 2.6 and 32 K. The analysis of the results indicates that the dephasing rate depends on quantum number v roughly quadratically. For a Morse oscillator this indicates that the coupling with lattice is dominated by the linear term with respect to the Morse oscillator coordinate. The quadratic term gives v dependence which is higher than quadratic. The longest dephasing times are most probably limited by inhomogeneous broadening which in our samples yields longest dephasing times up to ~300 ps for $v=2$. The temperature dependence of dephasing time and frequency shift shows that the main mechanism of coupling is via

pseudolocal modes with frequency in the 23–34-cm^{-1} range. The data at 2.6 K yield shorter dephasing times than at higher temperatures due to the change of morphology of the sample upon cooling and subsequent increase of inhomogeneous broadening.

ACKNOWLEDGMENTS

This work was supported by the Academy of Finland (decision no. 207044). Professor Henrik Kunttu and Professor Jouko Korppi-Tommola are warmly thanked for their support to this work.

[1] D. W. Oxtoby, Annu. Rev. Phys. Chem. **32**, 77 (1981).
[2] J. L. Skinner, Annu. Rev. Phys. Chem. **39**, 463 (1988).
[3] P. A. Madden and R. M. Lynden-Bell, Chem. Phys. Lett. **38**, 163 (1976).
[4] D. J. Diestler, Chem. Phys. Lett. **39**, 39 (1976).
[5] D. J. Diestler and A. H. Zewail, J. Chem. Phys. **71**, 3103 (1979).
[6] D. E. McCumber and M. D. Sturge, J. Appl. Phys. **34**, 1682 (1963).
[7] K. D. Rector and M. D. Fayer, in *Ultrafast Infrared and Raman Spectroscopy*, edited by M. D. Fayer (Marcel Dekker, New York, 2001).
[8] D. Hsu and J. L. Skinner, J. Chem. Phys. **81**, 5471 (1984).
[9] D. Hsu and J. L. Skinner, J. Chem. Phys. **83**, 2097 (1985).
[10] D. Hsu and J. L. Skinner, J. Chem. Phys. **83**, 2107 (1985).
[11] D. Hsu and J. L. Skinner, J. Chem. Phys. **87**, 54 (1987).
[12] P. DeBree and D. A. Wiersma, J. Chem. Phys. **70**, 790 (1979).
[13] R. M. Shelby, C. B. Harris, and P. A. Cornelius, J. Chem. Phys. **70**, 34 (1979).
[14] M. Karavitis, T. Kumada, I. Goldschleger, and V. A. Apkarian, Phys. Chem. Chem. Phys. **7**, 791 (2005).
[15] A. H. Zewail and D. J. Diestler, Chem. Phys. Lett. **65**, 37 (1979).
[16] M. R. Battaglia and P. A. Madden, Mol. Phys. **36**, 1601 (1978).
[17] A. B. Myers and F. Markel, Chem. Phys. **149**, 21 (1990).
[18] R. D. Coalson and D. G. Evans, Chem. Phys. **296**, 117 (2004).
[19] Q. Shi and E. Geva, J. Chem. Phys. **120**, 10647 (2004).
[20] M. Karavitis, R. Zadoyan, and V. A. Apkarian, J. Chem. Phys. **114**, 4131 (2001).
[21] M. Karavitis and V. A. Apkarian, J. Chem. Phys. **120**, 292 (2004).
[22] M. Karavitis, D. Segale, Z. Bihary, M. Pettersson, and V. A. Apkarian, Low Temp. Phys. **29**, 814 (2003).
[23] J. Tellinghuisen, J. Chem. Phys. **76**, 4736 (1982).
[24] J. Almy, K. Kizer, R. Zadoyan, and V. A. Apkarian, J. Phys. Chem. A **104**, 3508 (2000).
[25] B. W. F. Howard and L. Andrews, J. Raman Spectrosc. **2**, 442 (1974).
[26] R. Zadoyan and V. A. Apkarian, Chem. Phys. Lett. **326**, 1 (2000).
[27] S. Mukamel, *Principles of Nonlinear Spectroscopy* (Oxford University Press, New York, 1999).
[28] J. L. Skinner and D. Hsu, Chem. Phys. **128**, 35 (1988).
[29] J. A. C. Gallas, Phys. Rev. A **21**, 1829 (1980).
[30] Z. Bihary, M. Karavitis, R. B. Gerber, and V. A. Apkarian, J. Chem. Phys. **115**, 8006 (2001).
[31] M. E. Paige and C. B. Harris, Chem. Phys. **149**, 37 (1990).